Mechanisms of Fibrinogen Adsorption at Solid Substrates at Lower pH

ARTICLE *in* LANGMUIR · APRIL 2013

Impact Factor: 4.46 · DOI: 10.1021/la4012789 · Source: PubMed

4 AUTHORS:

Michal Ciesla
Jagiellonian University
41 PUBLICATIONS **287** CITATIONS
SEE PROFILE

Zbigniew Adamczyk
Akademickie Centrum Komputerowe CYFRON…
177 PUBLICATIONS **3,724** CITATIONS
SEE PROFILE

Jakub Barbasz
Instytut Katalizy i Fizykochemii Powierzchni i…
43 PUBLICATIONS **500** CITATIONS
SEE PROFILE

Monika Wasilewska
Instytut Katalizy i Fizykochemii Powierzchni i…
17 PUBLICATIONS **348** CITATIONS
SEE PROFILE

Langmuir

Article

pubs.acs.org/Langmuir

Mechanisms of Fibrinogen Adsorption at Solid Substrates at Lower pH

Michał Cieśla,[‡] Zbigniew Adamczyk,*[,†] Jakub Barbasz,[†,‡] and Monika Wasilewska[†]

[†]J. Haber Institute of Catalysis and Surface Chemistry, Polish Academy of Sciences, 30-239 Kraków, Niezapominajek 8, Poland

[‡]M. Smoluchowski Institute of Physics, Jagiellonian University, 30-059 Kraków, Reymonta 4, Poland

ABSTRACT: Adsorption of fibrinogen was theoretically studied using the three-dimensional random sequential adsorption (RSA) model. Fibrinogen molecule shape was approximated by the bead model considering the presence of flexible side arms. Various cases were considered *inter alia*, the side-on adsorption mechanisms and the simultaneous side-on/end-on adsorption mechanism. The latter mechanisms is pertinent to fibrinogen adsorption at lower pH (below isoelectric point of 5.8) where the entire molecule is positively charged. Extensive calculations enabled one to determine the jamming surface concentration (coverage) of molecules adsorbed under the side-on and end-on orientations as well as the total coverage. For the simultaneous side-on/end-on model the maximum surface concentration was 7.29×10^3 μm^{-2} corresponding to the protein coverage of 4.12 mg m^{-2} (without considering hydration). Additionally, the surface blocking functions for different adsorption regimes were determined and analytically approximated for the entire range of coverage by the interpolating polynomials. Using these blocking functions, fibrinogen adsorption kinetics for diffusion controlled transport conditions was evaluated. Comparison of these theoretical results with experimental data was made. It was demonstrated that the simultaneous side-on/end-on model properly reflects the maximum coverage of fibrinogen adsorbed on latex particles determined via the electrokinetic (electrophoretic mobility) and AFM measurements. Also, streaming potential measurements of fibrinogen adsorption kinetics on mica were successfully interpreted in terms of this model. The theoretical results derived in this work have implications for basic science providing information on mechanisms of anisotropic protein adsorption.

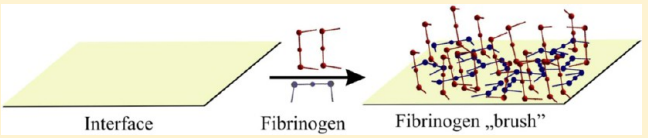

1. INTRODUCTION

Protein adsorption at solid interfaces is involved in cell adhesion, inflammatory response, thrombosis, artificial organ and biomaterial failure, plaque formation, fouling of membranes, etc. Additionally, controlled protein deposition on various surfaces is important for their efficient separation and purification by chromatography, filtration, for biocatalysis (enzyme immobilization), biosensing, immunological assays, etc.

Fibrinogen is one of the most extensively studied proteins because of its fundamental role in the blood clotting cascade, platelet adhesion, leucocyte binding, thrombosis, angiogenesis, inflammatory response, tumor growth, fouling of artificial organs, etc.[1−5]

Reliable information about fibrinogen's geometrical dimensions and conformations stem from the electron microscopic studies of Hall and Slayter[6] and others.[7−9] From the micrographs of fibrinogen adsorbed on mica, it was established that the molecule has a colinear, trinodular shape with a total length of 47.5 nm. The two equal end domains are spherical having a diameter of 6.5 nm; the middle domain has a diameter of 5 nm. These domains are connected by cylindrical rods, having a diameter of 1.5 nm. A schematic view of the fibrinogen molecule derived from the Hall-Slayter model, hereafter referred to as HS model, is shown in Table 1.

Similar shape and fibrinogen dimensions were confirmed by numerous studies carried out using atomic force microscopy (AFM).[10−16] Interestingly, the HS model shape and dimensions of fibrinogen agree with the true crystallographic shape derived from X-ray diffraction;[17] see Table 1.

As can be noticed, the fibrinogen molecule is highly anisotropic, characterized by considerable elongation (length to width ratio exceeding 10). However, in these works the shape and dimensions of fibrinogen were determined under dry or vacuum conditions, where the molecule is likely to change its native conformations occurring in the electrolyte solutions, because of considerable dehydration.

As far as the primary (chemical) structure is concerned, the fibrinogen molecule is a symmetric dimer composed of three identical pairs of polypeptide chains, referred to traditionally as Aα, Bβ, and γ chains.[9,18] They are coupled in the middle of the molecule through a few disulfide bridges forming a central nodule (see Table 1). The longest Aα chain is composed of 610 amino acids, the Bβ chain comprises 460 amino acids, and the γ chain 411 amino acids. Accordingly, the molar mass of the fibrinogen molecule equals 337 897 D.[19] Moreover, from the chemical structure it can be deduced that a considerable part of the Aα chains extends from the core of the molecule forming two polar appendages (arms) having each molar mass equal to 42 300 D.[20] Often, the end part of these the Aα appendages is

Received: April 4, 2013
Revised: April 26, 2013

   dx.doi.org/10.1021/la4012789 | *Langmuir* XXXX, XXX, XXX−XXX

Table 1. Model Shapes of the Fibrinogen Molecule

Model	Shape of Molecule	Remarks, Refs.
Hall and Slyter HS Model	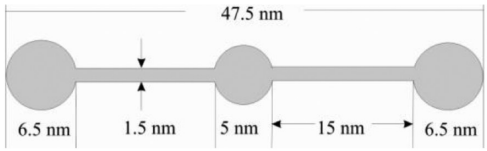	Ref. [6]
Chemical	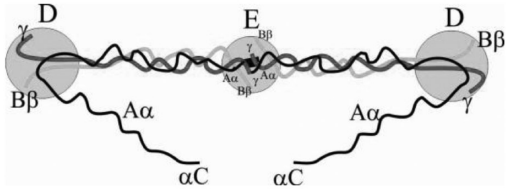	M_w = 337,897 Ref. [9, 18]
Crystallographic		$\bar{\nu}$ = 0.72 cm^3 g^{-1} ρ = 1.38 g cm^{-3} v = 405 nm^3 Ref. [17]
Bead Model B	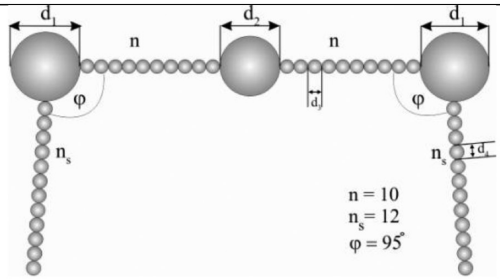	n = 10, n_s = 12 d_1 = 6.7 nm, d_2 = 5.3 nm, $d_3 = d_4$ = 1.5 nm Ref. [22]

called the αC domains.[14] These fragments of polypeptide Aα chains are collapsed under vacuum conditions and are not clearly visible in the crystallographic structure of fibrinogen (see Table 1). However, they play an essential role in the hydrodynamic behavior of the molecule under native conditions (in electrolyte solutions) because of heterogeneous charging of the molecule depending on pH and ionic strength. This was experimentally and theoretically demonstrated in refs 21 and 22. Two main conformations were predicted in these works: (i) the semicollapsed conformation appearing under physiological condition, i.e., pH 7.4 and the ionic strength of 0.15 M NaCl, where positive charge is located at the side chains and negative on the central nodule; and (ii) the expanded conformation prevailing for pH < 4, where the entire molecule becomes positively charged. These conformational changes and charge heterogeneity, induced by pH and ionic strength variations, are expected to influence mechanisms of fibrinogen adsorption at solid/electrolyte interfaces. However, despite a considerable significance of this problem, both from the practical and basic science point of view, remarkably few attempts were reported in the literature to theoretically analyze fibrinogen adsorption under various regimes.

This side-on adsorption mechanism was theoretically studied in ref 23 using the random sequential adsorption (RSA) model. The fibrinogen molecule shape was approximated by a string of 23 colinear touching spheres of various diameters forming a rigid and colinear configuration. However, the presence of side-arms was neglected in this model referred to hereafter as Model A of fibrinogen. It was predicted from these calculations that the maximum coverage of adsorbed fibrinogen under the side-on orientation was 1.4−1.7 mg m^{-2} (depending on the degree of hydration). This result was consistent with experimental results of Bai et al.[24] who measured fibrinogen adsorption on various substrates such as stainless steel, nickel−titanium alloy, and pure titanium. The amount of adsorbed fibrinogen was determined using the *ex situ* wavelength dispersive spectroscopy (WDS). In the case of the stainless steel substrate the maximum coverage of fibrinogen was 1.40 mg m^{-2}. In the case of the nickel−titanium alloy the maximum coverage was 1.70 mg m^{-2}.

dx.doi.org/10.1021/la4012789 | *Langmuir* XXXX, XXX, XXX−XXX

However, there are many reports in the literature indicating that the maximum coverage of fibrinogen for other surfaces can attain larger values. For example, Malmsten,[25] using ellipsometry, determined the kinetics of fibrinogen adsorption on methylated silica at pH = 7.4 and I = 0.15 M. The coverage of fibrinogen varied from 4 to 5 mg m^{-2} for a fibrinogen bulk concentration changed from 50 to 1000 mg L^{-1} (parts per million).

Precise kinetic measurements of fibrinogen adsorption on silicon and modified glass surfaces forming parallel-plate channels were performed by Santore et al.[26,27] using the *in situ* fluorescent TIRF technique. These results were supplemented with an interesting AFM determination of the kinetics of fibrinogen adsorption. The maximum coverage of fibrinogen determined in these works was 3.8−4.8 mg m^{-2} for the bulk concentration of fibrinogen varying between 25 and 100 mg L^{-1}. In ref 27 an interesting study of fibrinogen spreading kinetics at hydrophobic and hydrophilic self-assembled surfaces deposited on microscope slides was performed. Whereas the footprint area on the hydrophilic surface remained fairly stable in time (equal to 160 nm^2) for the hydrophobic surface the footprint are considerably increased (up to 400 nm^2) over the period of 2 h. This was interpreted as an energy barrier controlled rearrangement of adsorbed fibrinogen molecules to a more stable, side-on configuration.

Ellipsometric measurements of fibrinogen adsorption on silicon plates were performed by Ortega −Vinuesa et al.[10,11] (for bulk protein concentration of 70 mg L^{-1}). For pH = 4, the maximum coverage varied between 2 and 3.8 mg m^{-2}, for the ionic strength of 2×10^{-3} and 5×10^{-2} M, respectively.

Recently, Kalasin and Santore,[28] using the TIRF method, studied adsorption of fibrinogen on modified glass slides converted to silica. They determined that the maximum coverage varied between 2 and 4 mg m^{-2} for ionic strength ranging between 0.176 and 0.005 M (pH = 7.4, fibrinogen bulk concentration 25 mg L^{-1}).

In ref 29 fibrinogen adsorption on latex particles was studied using the microelectrophortic and solution depletion methods. The roles of ionic strength and pH were evaluated. It was determined that for pH 3.5 the maximum coverage varied between 2 and 3.6 mg m^{-2} for ionic strength changed between 1×10^{-3} and 0.15 M NaCl.

In ref 30 theoretical simulations were performed in order to account for the experimentally measured higher coverages of fibrinogen. It was assumed that initially fibrinogen molecules adsorb side-on, but for longer adsorption times, after completing the side-on monolayer, they can also adsorb under the end-on orientation. This adsorption regime seems plausible because of a considerably smaller surface area demand for this fibrinogen orientation. However, in these calculations the simple HS Model of fibrinogen was used, hence the role of the side arms could not be properly accounted for.

Therefore, the aim of this work is a thorough theoretical analysis of possible adsorption mechanisms of fibrinogen at lower pH range below the isoelectric point, where the entire molecule bears a net positive charge. As an extension of previous approaches,[30] a more refined Model B (see Table 1) of fibrinogen is used where the presence of side arms is explicitly taken in to account. Accordingly, fibrinogen adsorption is treated in a more realistic way as a three-dimensional process. The main results of this work are the accurate jamming coverages for various adsorption regimes of fibrinogen and the surface blocking functions (referred often to as the available surface function ASF). This allows one to quantitatively predict fibrinogen adsorption kinetics under various transport conditions (diffusion and convection) and properly interpret experimental results.

Besides being significant for a complete description of fibrinogen adsorption at lower pHs, these theoretical results also have implications for basic science, providing reliable information about mechanisms of anisotropic molecule adsorption on heterogeneous surfaces.

2. SIMULATION PROCEDURE

In this work, adsorption of fibrinogen was analyzed in terms of the RSA model. This is a stochastic process in which objects (particles, molecules) are consecutively placed on homogeneous surfaces without penetrating into any previously adsorbed object.[31−41] They can only adsorb after contacting an uncovered surface area of the interface, hereafter referred to as the collector. Hence, the process is completed if there is no available (uncovered) collector surface area to accommodate the object under a prescribed orientation. This final coverage is called the jamming coverage and represents the most relevant parameter determined in RSA simulations.

The RSA approach has widely been used to perform calculations for continuous, homogeneous surfaces and spherical particles.[31−35] Fewer results exist for anisotropic (elongated) particle adsorption such as cylinders,[36] spheroids, and spherocylinders.[37,38] A three-dimensional (unoriented) adsorption regime of prolate and oblate spheroids was analyzed in ref 39.

In previous work,[23,30] the RSA model was applied to theoretically describe the irreversible, side-on, and end-on adsorption of fibrinogen on homogeneous substrates.

In this work, we analyze adsorption mechanisms of fibrinogen using a more refined bead Model B (see Table 1) where the presence of side arms is explicitly taken in to account. In terms of this model, the real shape of the fibrinogen molecule is replaced by a string of colinear touching spheres of various diameters. The two external spheres have diameters of 6.7 nm and the central sphere has a diameter of 5.3 nm. The remaining 20 spheres of equal size have diameters of 1.5 nm. The side arms are made of straight sequences of n_s beads of equal size, having the diameter of d_4. These arms form the angle φ with the main body of the fibrinogen molecule. In calculations performed in this work, the angle φ was a variable parameter, which allowed one to theoretically study the influence of fibrinogen conformations on the jamming coverage and blocking functions. The number of beads in the side chains was fixed at n_s = 12, which gives the side-on cross-section area of the molecule S_g equal to 170 nm^2.

Recently, this bead Model B was exploited to calculate hydrodynamic resistance tensors, diffusion coefficients, intrinsic viscosities, and conformations of fibrinogen under various physicochemical conditions.[22]

Simulations for such model fibrinogen molecules were carried out according to the RSA scheme described elsewhere[23,30] for interfaces (collectors) having a square shape of the size L_c, of 2000 to 5000 nm. At the periphery of the collector, the no-penetration boundary conditions were applied, i.e., the molecule could only adsorb if the centers of all spheres forming the model molecule were within the simulation area.

The mains steps of the RSA simulation algorithm used in this work were as follows:

dx.doi.org/10.1021/la4012789 | *Langmuir* XXXX, XXX, XXX−XXX

Table 2. Adsorption Models and Allowed Configurations of Fibrinogen upon Adsorption

Model	Allowed Configurations	Remarks
1. Side-on without crossings	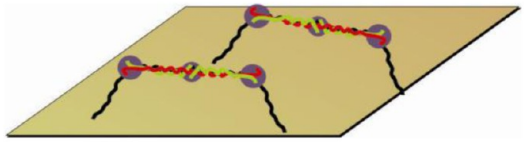	Irreversible (no overlapping)
2. Side-on with crossings	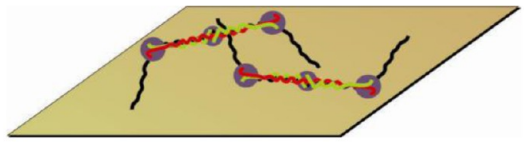	Irreversible (crossings)
3. Side-on with crossings, afterwards end-on	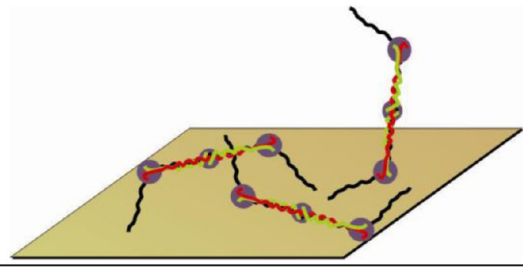	Irreversible side-on, Irreversible end-on
4. Side-on, end-on, simultaneously	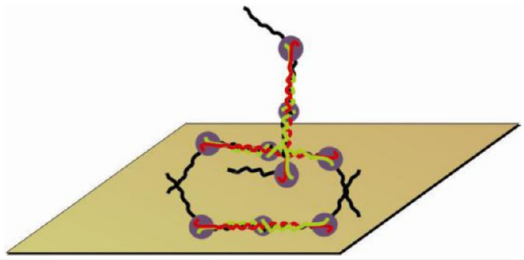	Irreversible side-on, Irreversible end-on

(i) An attempt at adsorbing a virtual fibrinogen molecule is done by choosing at random its orientation and position over the homogeneous collector.
(ii) An overlapping test is performed by checking if the surface to surface distance between any of the spheres of different molecules was not smaller than zero. The efficiency of the overlapping test was increased using a subsidiary matrix containing information about previously adsorbed particles in the vicinity of the virtual one.
(iii) If there is no overlapping, the virtual molecule becomes irreversibly adsorbed. Its position and orientation remain unchanged during the course of calculations.
(iv) If there is overlapping, a new adsorption attempt is done, uncorrelated with previous attempts.

Using this general scheme, four main adsorption mechanism of fibrinogen were thoroughly analyzed (see Table 2):

(i) the purely side-on adsorption mechanism where fibrinogen molecules could adsorb if both the external spheres and both arms touch the collector surface.
(ii) the side-on adsorption mechanism with crossings where both the external spheres (diameter d_1) touch the collector surface but the arms are allowed to cross over other molecules in space.
(iii) the side-on adsorption mechanism with crossings in the first stage until the jamming coverage is attained and afterward, in the second stage, the end-on adsorption of additional molecules in the free spaces (holes) among side-on adsorbed molecules.
(iv) the side-on and end-on adsorption occurring simultaneously (the side-on is considered first but if there is not enough space the virtual molecule can adsorb end-on). This is also referred to hereafter as the simultaneous side-on/end-on adsorption mechanism.

The two first mechanisms seem adequate for fibrinogen adsorption at low ionic strength where the lateral repulsion among molecules prohibits the appearance of the end-on configurations.

dx.doi.org/10.1021/la4012789 | Langmuir XXXX, XXX, XXX−XXX

The third mechanism is expected to properly reflect the situation for pH close to the protein isoelectric point (pH 5.8) and higher ionic strength where the fibrinogen molecules can only be irreversibly adsorbed in the side-on orientation and the end-on adsorption remains reversible.

On the other hand, the fourth mechanism is pertinent to lower pH where fibrinogen molecules are positively charged, hence they can adsorb irreversibly on negatively charged surfaces in both the side-on and end-on orientations because of a large (negative) binding energy. It is also plausible that this mechanism is pertinent to fibrinogen adsorption on hydrophobic surfaces at wider pH range because the binding energy is generally higher than for hydrophilic surfaces.[27]

The primary information derived from these simulations is the number of adsorbed molecules, in the side-on $N_{p\parallel}$ and the end-on $N_{p\perp}$ configurations, determined as a function of the total number of attempts N_{att}. By knowing this parameter, the surface concentration of molecules can be calculated as

$$N = N_p/S_c \tag{1}$$

where $S_c = L_c^2$ is the geometrical area of the collector.

It is useful for analyzing asymptotic adsorption regimes to introduce the dimensionless coverage defined as[23,30]

$$\theta = S_g N \tag{2}$$

where S_g is the geometrical cross-section area of the bead model of fibrinogen.

The blocking function (available surface function-ASF) was determined for a fixed fibrinogen coverage from the constitutive dependence

$$B(\theta) = 1/N_{att} \tag{3}$$

Where N_{att} is the number of attempts at adsorbing the fibrinogen molecule over the interface covered to the degree of θ.

By definition, under the jamming state, the ASF function vanishes, so

$$B(\theta_\infty) = 0 \tag{4}$$

where θ_∞ is the jamming coverage of the monolayer, which is the most relevant parameter derived from the simulations.

The dimensionless time in an individual adsorption run is defined as[23]

$$\tau = N_{att} S_g/S_c \tag{5}$$

where N_{att} is the actual number of adsorption attempts in the run.

To obtain proper statistics, simulations were performed for an large number of collectors, with the total number of generated fibrinogen molecules of the order of 10^6.

3. RESULTS AND DISCUSSION

3.1. Calculations of the ASF Function and the Jamming Coverage. The main goal of calculations performed in this work was determining the jamming coverages, blocking functions, and adsorption kinetics of fibrinogen for the above adsorption regimes.

Accordingly, in the first stage of simulations, the fibrinogen monolayers of a desired coverage were generated according to the above-described algorithm. Snapshots of monolayers derived in these simulations for the side-on and the simultaneous side-on/end-on adsorption regimes are shown in Figures 1,2 for N varying between 500 and 2000 μm^{-2}. As can be observed, in the case of the simultaneous adsorption, the

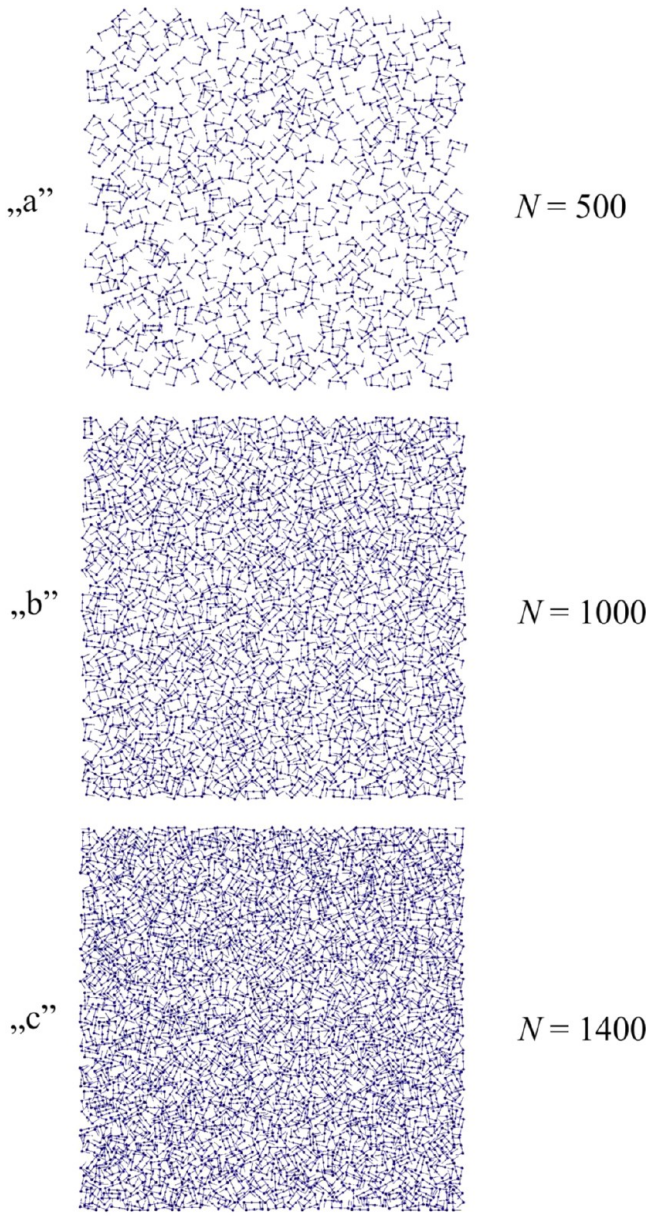

Figure 1. Snapshots of the fibrinogen monolayers derived from the RSA simulations. Side-on adsorption mechanisms with crossings, φ = 95°. Part a: N = 500 μm^{-2}. Part b: N = 1000 μm^{-2}. Part c: N = 1400 (jamming coverage).

number of molecules adsorbed in the end-on configuration (marked in red) prevails over the side-on population (marked in blue). This leads to formation of a brush-like fibrinogen monolayer for N > 500 μm^{-2}. Quantitatively this effect is shown in Figure 3, where the dependencies of the surface concentration of molecules in the side-on and end-on orientations are plotted as a function of the surface concentration of all adsorbed molecules N. As can be seen, for N < 700 μm^{-2} the number of fibrinogens in the side-on configuration is larger than the number of molecules in the end-on conformations. For the sake of convenience the numerical results shown in Figure 3 were interpolated by the following polynomials valid for N < 10^3 μm^{-2}.

dx.doi.org/10.1021/la4012789 | Langmuir XXXX, XXX, XXX−XXX

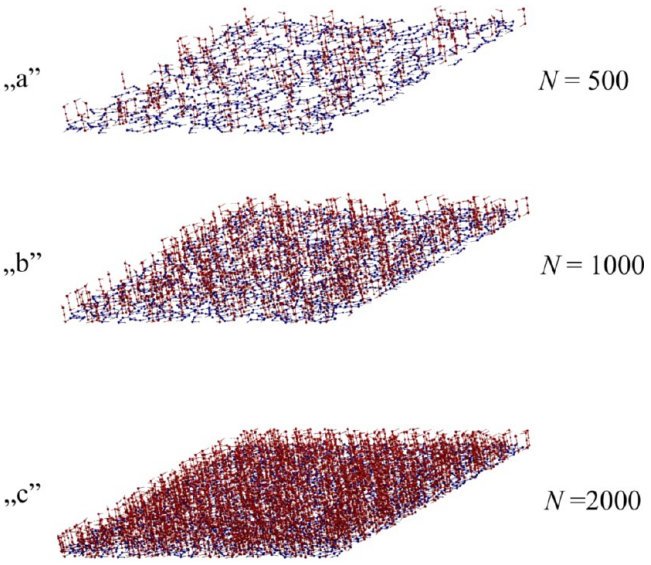

Figure 2. Snapshots of the fibrinogen monolayers derived from the RSA simulations for the simultaneous side-on/end-on adsorption, φ = 95°. Part a: N = 500 μm $^{-2}$. Part b: N = 1000 μm $^{-2}$. Part c: N = 2000 μm^{-2}. Molecules adsorbed in the end-on configurations are plotted in red color and molecules adsorbed in the side-on configuration are plotted in blue color.

$$N_{\perp} = c_1 N + c_2 N^2 - c_3 N^3$$
$$N_{p\parallel} = (1 - c_1) N - c_2 N^2 + c_3 N^3 \quad (6)$$

where

$$c_1 = 0.044, \quad c_2 = 9.31 \times 10^{-4}, \quad c_3 = 3.333 \times 10^{-7}$$
(simultaneous side-on/end-on adsorption, $\varphi = 115°$)

$$c_1 = 0.036, \quad c_2 = 9.00 \times 10^{-4}, \quad c_3 = 3 \times 10^{-7}$$
(simultaneous side-on/end-on adsorption, $\varphi = 95°$) (7)

Analogous interpolations were derived for 10^3 μm^{-2} < N < 7 × 10^3 μm^{-2}; see Figure 3 part b

$$N_{\perp} = c'_0 + c'_1 (N - 1000)$$
$$N_{p\parallel} = 1 - N_{\perp} \quad (8)$$

where

$$c'_0 = 619.3, \quad c'_1 = 0.988$$
(simultaneous side-on/end-on adsorption, $\varphi = 115°$)

$$c'_0 = 606, \quad c'_1 = 0.987$$
(simultaneous side-on/end-on adsorption, $\varphi = 95°$) (9)

It should be mentioned that the higher angle φ corresponds to an average fibrinogen conformation predicted for lower ionic strength and φ = 95° corresponds to the molecule conformation at high (physiological) ionic strength.[22]

As can be observed in Figure 3 the influence of this parameter on fibrinogen adsorption (the $N_{\perp}$ vs N dependencies) is rather minor.

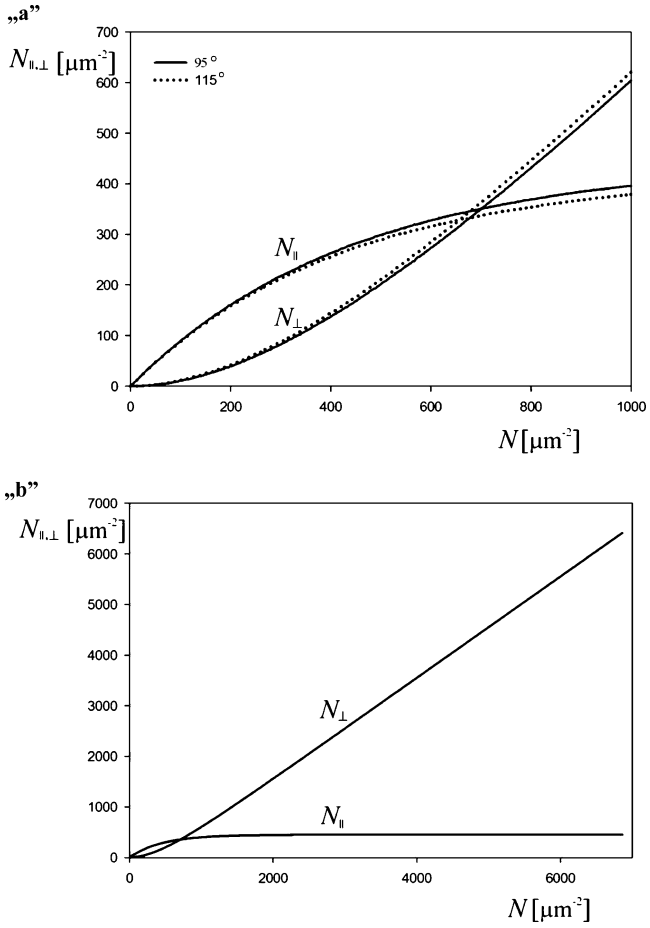

Figure 3. Dependence of surface concentration of fibrinogen molecules in the side-on $N_{\parallel}$ and the end-on $N_{\perp}$ orientations, on the total surface concentration $N = N_{\perp} + N_{\parallel}$ derived from the RSA simulations for the simultaneous adsorption regime. Part a: low surface concentration range. Part b: high concentration range. The solid lines denote the smoothened numerical results calculated from eqs 6–9 for φ = 95° and the dashed line for φ = 115°.

It should also be noted that in the RSA simulations one cannot directly determine the true jamming surface concentrations because this would require an infinite number of attempts. However, these parameters can be precisely calculated by the interpolation procedure developed in refs 37. The method is based on the use of the asymptotic form of the equation describing particle adsorption in the limit of large number of attempts (simulation time)

$$N_{\infty} = N_L + C_N N_{att}^{-1/l} \quad (10)$$

where N_{∞} is the true jamming surface concentration for the infinite number of attempts, N_L is the surface concentration for a large (but finite) number of attempts, and C_N and l are parameters determined from the RSA simulations. For spherical particles it is theoretically predicted that l = 2[31−34] whereas for anisotropic particles the exponent should be equal to 3.[37]

Equation 10 can be used for efficient extrapolation of results obtained for long, but finite simulation times to infinite times, impractical to attain. It was confirmed in our simulations that eq 10 adequately reflects the numerical results for l = 3 and various adsorption mechanisms. In this way, the jamming surface concentrations of fibrinogen N_{∞} were derived, which are quantities of a primary significance for interpretation of

dx.doi.org/10.1021/la4012789 | Langmuir XXXX, XXX, XXX−XXX

Table 3. Jamming Coverages for Fibrinogen Model B Derived from the RSA Simulations[a]

	φ = 115°					φ = 95°				
Adsorption model	$N_{\parallel\infty}$ [μm^{-2}]	$N_{\perp\infty}$ [μm^{-2}]	N_∞ [$_{\mu m}^{-2}$]	F [nm^2]	Γ_∞ [mg m^{-2}]	$N_{\parallel\infty}$ [μm^{-2}]	$N_{\perp\infty}$ [μm^{-2}]	N_∞ [$_{\mu m}^{-2}$]	F [nm^2]	Γ_∞ [mg m^{-2}]
Side-on without crossings	972	-	972	1030	0.545	932	-	932	1070	0.523
Side-on with crossings	1400	-	1400	714	0.785	1460	-	1460	686	0.819
Side-on with crossings, afterward end-on	1400	4070	5470	183	3.07	1460	3980	5440	184	3.05
Side-on/end-on simultaneously	428	6960	7390	135	4.15	448	6900	7340	136	4.12

[a] $N_{\parallel\infty}$ - side-on fraction. $N_{\perp\infty}$ - end-on fraction. N_∞ - total = side-on + end-on fraction. $\Gamma_\infty = 10^{15}\,(M_w/Av)\,N_\infty$. $F = 10^6/N_\infty$.

experimental results. This is so, because, contrary to the coverage, the surface concentrations N_∞ are independent of the choice of the cross-section area of the molecule. Values of the maximum coverages derived from our simulations for the above-mentioned adsorption mechanisms are

$$N_\infty = 1.40 \times 10^3 \mu m^{-2} \quad \text{(side-on adsorption with crossings, } \varphi = 115°)$$

$$N_\infty = 1.46 \times 10^3 \mu m^{-2} \quad \text{(side-on adsorption with crossings, } \varphi = 95°)$$

$$N_\infty = 7.39 \times 10^3 \mu m^{-2} \quad \text{(simultaneous side-on/end-on adsorption, } \varphi = 115°)$$

$$N_\infty = 7.34 \times 10^3 \mu m^{-2} \quad \text{(simultaneous side-on/end-on, } \varphi = 95°) \qquad (11)$$

These and other values calculated for various adsorption mechanism are listed in Table 3. For the sake of convenience, in Table 3 the 'footprint' areas are also given, often used by analyzing experimental data.[26] The footprint area F (expressed in nm^2) is connected with the surface concentration (expressed in μm^{-2}) via the simple relationship $F = 10^6/N$.

It is interesting in the latter case (simultaneous adsorption) to split the total surface concentration of molecules N_∞ into the side-on and end-on components, which are 428 and 6965 μm^{-2}, respectively. As can be noted, under the jamming state, the number of molecules in the end-on conformation significantly exceeds the number of molecules in the side-on population.

The influence of the angle φ on the jamming coverage was studied in more detail. The results shown in Figure 4 indicate that the changes in the jamming surface concentrations of fibrinogen were less than 2% if the angle was varied between 95° and 130°, which covers the practically occurring conformations of fibrinogen.[22]

Knowing the surface concentrations, one can calculate via eq 2 the dimensionless coverage of molecules, which is a more convenient parameter for expressing blocking functions and analyzing adsorption kinetics. The blocking functions for a discrete set of coverages were determined using eq 3. Averages from 10 to 20 collectors were taken, typically having the size of 5000 × 5000 nm for lower coverage range, $\Theta < 0.05$. For higher coverage, the size of the collector was typically 2000 × 2000 nm. It was determined from these calculations that for the lower coverage range the ASF function could be well approximated by the polynomial expansion

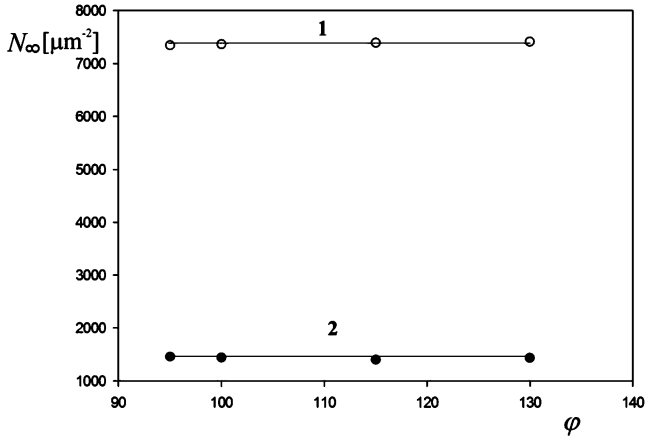

Figure 4. Dependence of the jamming surface concentration of fibrinogen $N_\infty = (N_{\parallel\infty} + N_{\perp\infty})$ on the angle φ derived from the RSA simulations. 1: the simultaneous adsorption. 2: the side-on adsorption with crossings. The solid lines denote the smoothened numerical results.

$$B(\Theta) = 1 - C_1\Theta + C_2\Theta^2 - C_3\Theta^3 + 0(\Theta^4) \qquad (12)$$

where C_1, C_2, and C_3 are the dimensionless constants, which assume the following values for the various adsorption regimes:

$$C_1 = 21.78, \quad C_2 = 122.7, \quad C_3 = 10.80 \quad \text{(side-on adsorption with crossings, } \varphi = 115°)$$

$$C_1 = 20.54, \quad C_2 = 106.4, \quad C_3 = 11.82 \quad \text{(side-on adsorption with crossings, } \varphi = 95°)$$

$$C_1 = 7.50, \quad C_2 = 23.93, \quad C_3 = -22.44 \quad \text{(simultaneous side-on/end-on adsorption, } \varphi = 115°)$$

$$C_1 = 7.51, \quad C_2 = 23.55, \quad C_3 = -19.52 \quad \text{(simultaneous side-on/end-on, } \varphi = 95°) \qquad (13)$$

As can be seen in Figure 5a, in the case of the simultaneous adsorption, the expansion, given by eq 12, well reflects the exact numerical data for $\Theta < 0.2$ where $B(\Theta)$ decreases to 0.3. It should also be mentioned that the function derived from first-order expansion $B(\Theta) = 1 - C_1\Theta$, which corresponds to the pseudo-Langmuirian model, only gives a reasonable approximation of the exact data for $\Theta < 0.05$.

Determination of the blocking functions for higher coverage range is more tedious, because the available surfaces exist in the form of isolated targets of very small surface areas.[33,34] Moreover, in the case of anisotropic objects such as fibrinogen, these targets are selective because a specific orientation of the

dx.doi.org/10.1021/la4012789 | Langmuir XXXX, XXX, XXX−XXX

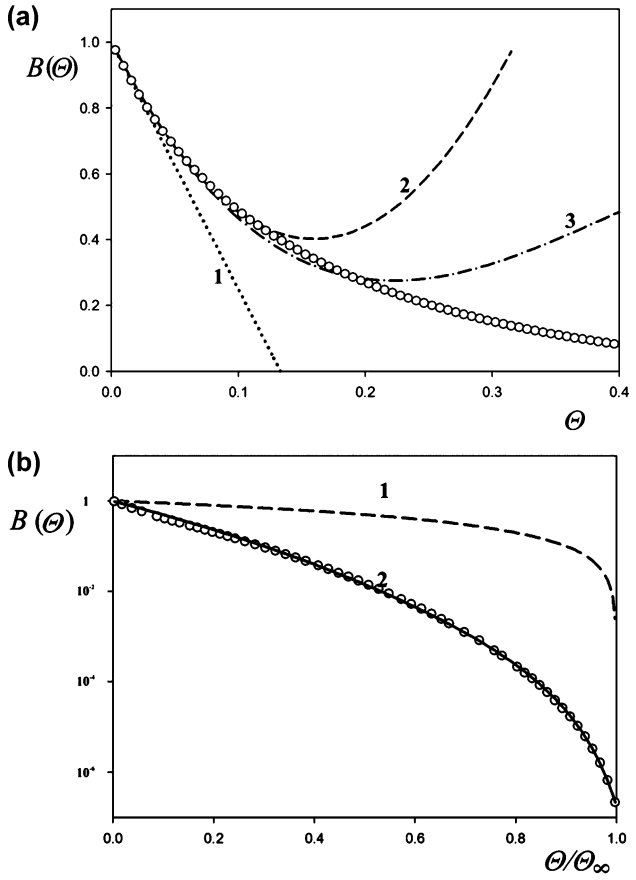

Figure 5. Dependence of the surface blocking function $B(\Theta)$ on the fibrinogen coverage $\Theta = S_g N$, derived from the RSA simulations for the simultaneous adsorption, $\varphi = 95°$. Part a: the low coverage range. The points denote the numerical results derived from the RSA simulations and the lines 1−3 are analytical fits: 1: $B(\Theta) = 1 - C_1\,\Theta$. 2: $B(\Theta) = 1 - C_1\,\Theta + C_2\,\Theta^2$. 3: $B(\Theta) = 1 - C_1\,\Theta + C_2\,\Theta^2 - C_3\,\Theta^3$. Part b: the high low coverage range. The points denote the numerical results derived from the RSA simulations and the lines denote analytical approximations calculated as: (1) $B(\Theta) = 1 - C_1\,(\Theta/\,\Theta_\infty)$ (pseudo-Langmuirian model); (2) $B(\Theta)$ calculated from eq 17.

adsorbing molecule is required to fit into the available surface areas.[37,38] In order to derive asymptotic expressions for this adsorption regime one can use eq 10 that can be expressed in terms of the coverage and the dimensionless time (defined by eq 5) in the following form

$$\Theta_\infty = \Theta_L + C_\infty \tau^{-1/3} \tag{14}$$

where Θ_L is the coverage for $\tau \gg 1$, $\Theta_\infty = S_g N_\infty$ is the true jamming coverage for the infinite time and C_∞ is the dimensionless constant. Equation 14 can be used for an efficient extrapolation of results obtained for long, but finite simulation times to infinite times, impractical to attain.

It was confirmed in our simulations that eq 14 adequately reflects the numerical results for $\tau^{-1/3} < 0.1$ ($\tau > 10^3$) and various adsorption mechanisms. By proving this one can derive asymptotic forms by noting that the blocking functions are connected with the rate of particle adsorption through the constitutive dependence[33,34]

$$B(\Theta) = \frac{d\Theta}{d\tau} \tag{15}$$

Using eq 14 one can show that the ASF function for fibrinogen for high coverage range assumes the form

$$B(\Theta) = C'_\infty (1 - \bar{\Theta})^4 \tag{16}$$

where $\bar{\Theta} = \Theta/\Theta_\infty$ is the normalized coverage and $C'_\infty = 1/(3\,\Theta_\infty^2 C_\infty^3)$.

Explicitly, these constants are 0.017 for the side-on adsorption and 0.058 for the simultaneous side-on/end-on adsorption (independently, of the angle φ). As can be seen, the C'_∞ constants are much smaller than unity; one can deduce that the blocking functions for all adsorption regimes vanish rapidly for the coverage approaching jamming limits.

Knowing the exact expressions for blocking functions in the limits of low and high coverage, one can approximate them by the useful, polynomial expression

$$B(\Theta) = (1 + a_1\bar{\Theta} + a_2\bar{\Theta}^2 + a_3\bar{\Theta}^3)(1 - \bar{\Theta})^4 \tag{17}$$

The coefficients of the series expansion appearing in eq 17 for various adsorption regimes are

$$\begin{aligned}
&a_1 = -2.751, \quad a_2 = 2.495, \quad a_3 = -0.722 \\
&\quad \text{(side-on adsorption with crossings,} \quad \varphi = 115°) \\
&a_1 = -2.632, \quad a_2 = 2.233, \quad a_3 = -0.577 \\
&\quad \text{(side-on adsorption with crossings,} \quad \varphi = 95°) \\
&a_1 = -3.017, \quad a_2 = 3.431, \quad a_3 = -1.413 \\
&\quad \text{(simultaneous side-on/end-on adsorption,} \quad \varphi = 115°) \\
&a_1 = -3.064, \quad a_2 = 3.527, \quad a_3 = -1.461 \\
&\quad \text{(simultaneous side-on/end-on,} \quad \varphi = 95°)
\end{aligned} \tag{18}$$

The analytical expression for $B(\Theta)$ derived from the interpolating formula eq 17 is compared in Figure 5b with the numerical results derived from the RSA simulations for the simultaneous adsorption regime. As can be seen, the interpolating function matches the exact numerical data for the entire range of coverage well up to the jamming limit. It is also interesting to observe that the function derived from the Langmuir model, assuming $B(\Theta) = 1\text{-}\Theta$, is inadequate for the entire range of coverage considerably overestimating the numerical data.

One can, therefore, conclude that, because of its closed form and proper asymptotics for high and low coverage, the interpolating function given by eq 17 is convenient to use in numerical calculations of fibrinogen adsorption kinetics presented below.

3.2. Calculations of Fibrinogen Adsorption Kinetics and Comparison and with Experiments. Knowing the blocking functions and jamming coverage, one can calculate adsorption kinetics of fibrinogen under various transport mechanisms. This can be done using the previously developed approach based on the continuity (mass-balance) equation describing molecule transfer through the boundary layer under irreversible adsorption conditions[40,41]

$$\frac{1}{S_g}\frac{d\Theta}{dt} = j_a = k_a n(\delta_a) B(\Theta) \tag{19}$$

where t is the time, j_a is the adsorption flux, k_a is the adsorption constant, and $n(\delta_a)$ is the number concentration of particles at the adsorption boundary layer of the thickness δ_a.

dx.doi.org/10.1021/la4012789 | Langmuir XXXX, XXX, XXX−XXX

Equation 19 is coupled with the bulk mass transfer equation and both should be simultaneously solved.[40,41] In the case of convection driven transport (flow) the molecule concentration at the edge of the adsorption layer $n(\delta_a)$ remains in a quasi-equilibrium with the surface coverage, which is the effect of short relaxation compared to the surface coverage variations.[40] Therefore, in this case, eq 19 can be transformed to the convenient form

$$j_a = k_c n_b \frac{KB(\Theta)}{(K-1)B(\Theta)+1} \tag{20}$$

where $K = k_a/k_c$ is the dimensionless coupling constants and k_c is the bulk transfer rate constant, known in analytical form for many types of flows and interface configurations.[40]

Equation 20 can be integrated to the useful form

$$\int_0^{\Theta'} \frac{(K-1)B(\Theta')+1}{KB(\Theta')} \mathrm{d}\Theta' = t/t_{ch} = \tau \tag{21}$$

where $t_{ch} = 1/(S_g k_c n_b)$ is the characteristic time of particle monolayer formation under the convection transport and τ is the dimensionless time that corresponds to the above-defined via eq 5 simulation time.

Equation 21 represents the general solution for the particle deposition kinetics under convection driven transport. It can be explicitly evaluated by numerical integration using the above derived blocking functions by considering that, for the barrier-less adsorption regime, the adsorption constant is given by[40]

$$k_a = \frac{D}{\delta_a} \Big/ \left[1 + \frac{1}{2} \ln \delta_a/\delta_m\right] \tag{22}$$

where δ_m is the minimum distance between the molecule and the interface and D is the protein diffusion coefficient.

In the case of the diffusion-controlled transport, the situation becomes more complicated because the constitutive expression for the flux, eq 19 cannot be directly integrated since the bulk flux remains nonstationary for all times. Therefore, in order to calculate the coverage explicitly, one has to solve the bulk diffusion equation with eq 19 as applied as the kinetic boundary condition. This has been extensively discussed in previous work.[23,30] As demonstrated, the solutions of this boundary value problem can be derived by the finite-difference numerical method. The solution is facilitated by introducing the dimensionless time and the adsorption constant

$$\tau = t/t_{ch} = t(D S_g^2 n_b^2)$$
$$\bar{k}_a = k_a/(S_g D n_b) \tag{23}$$

It is instructive to calculate the characteristic time $t_{ch} = 1/(DS_g^2 n_b^2)$ and $\bar{k}_a$ pertinent to fibrinogen adsorption on solid interfaces. Considering that $D = 2.1 \times 10^{-11}$ m^2 s^{-1} (experimental value at $T = 293$ K[22]), $\delta_m = 0.5$ nm, $\delta_a = 21$ nm (hydrodynamic diameter of fibrinogen), $S_g = 137$ nm^2 (footprint area for the simultaneous adsorption), and the bulk fibrinogen concentration of 1 mg L^{-1} (1.78×10^{18} m^{-3}), $t_{ch} = 7.99 \times 10^5$ s (221 h), $\bar{k}_a = 6.80 \times 10^4$. For $n_b = 100$ mg L^{-1} (1.78×10^{20} m^{-3}) which is the highest value used in kinetic experimental measurements, $t_{ch} = 79.9$ s, $\bar{k}_a = 6.80 \times 10^2$. This estimation unequivocally shows that, for this range of fibrinogen concentration the kinetics runs are long-lasting processes, facilitating experimental measurements.

Theoretical results calculated in the case of diffusion-controlled transport of fibrinogen for the simultaneous adsorption are shown in Figure 6 for $\bar{k}_a = 6.80 \times 10^3$ and $\bar{k}_a = 6.80 \times 10^2$. This corresponds, to the bulk concentration of fibrinogen suspension 10 and 100 mg L^{-1}, respectively. These data were derived by numerical integration of the bulk diffusion equation with eq 19 as the boundary condition using the implicit Crank-Nicholson finite difference scheme.[23,30] For the sake of convenience the Θ/Θ_∞ vs the square root of the reduced time $(t/t_{ch})^{1/2}$ coordinate system is used. As can be seen, fibrinogen coverage for t/t_{ch} smaller than unity increases linearly with $(t/t_{ch})^{1/2}$, according to the equation

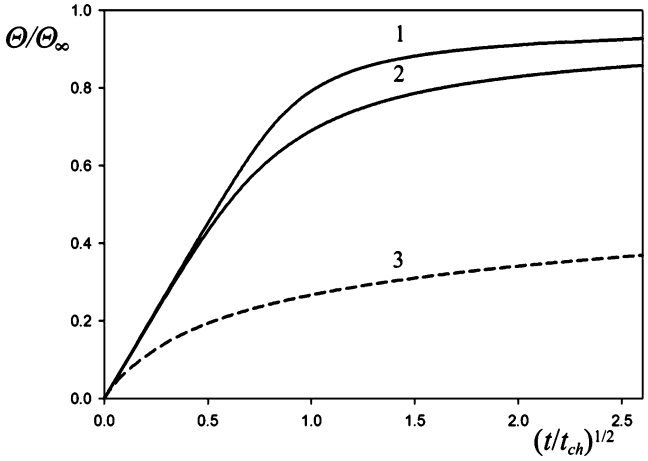

Figure 6. Kinetics of fibrinogen adsorption on the square root of the normalized time $(t/t_{ch})^{1/2}$ calculated for the diffusion-controlled deposition regime and the simultaneous adsorption regime, $\varphi = 95°$. The solid lines denote exact theoretical results calculated by solving the diffusion equation for the bulk fibrinogen concentration of (1) c_b = 10 mg L^{-1}; (2) c_b = 100 mg L^{-1}. The dashed line (3) shows the results calculated using the standard RSA model, assuming a surface controlled-regime (where the molecule flux is reduced by the factor $B(\theta)$).

$$\Theta/\Theta_\infty = 2(\tau/\pi)^{1/2}/\theta_\infty \tag{24}$$

In terms of dimensional variables, eq 24 can be expressed as

$$N = 2(Dt/\pi)^{1/2} n_b \tag{25}$$

As can be observed in Figure 6, eq 24 remains valid until the coverage approached 0.5 of the jamming coverage. This indicates that the surface transport resistance stemming from blocking effects plays a negligible role in comparison with the bulk transport resistance.

On the other hand, for long adsorption times, where the particle coverage approaches the jamming limit, the overall particle adsorption rate is governed by the transport in the adsorption layer. In this case one can integrate eq 19 assuming $n(\delta_a) = 1$ that results in the expression

$$\Theta_\infty = \Theta_L + C_\infty(\bar{k}_a\tau)^{-1/3} = \Theta_L + C_\infty(S_g k_a n_b t)^{-1/3} \tag{26}$$

where Θ_L is the coverage experimentally determined for long times and C_∞ is the dimensionless constant equal to 1.55 for the simultaneous adsorption.

As can be deduced from eq 26, for a fixed adsorption time, the jamming coverage is asymptotically attained as $n_b^{-1/3}$, i.e., in a very inefficient manner. Therefore, quite significant errors

dx.doi.org/10.1021/la4012789 | Langmuir XXXX, XXX, XXX−XXX

may appear if the experimental data obtained for long times are accepted as true jamming coverages. In order to obtain correct results, eq 26 should be used to extrapolate these long-time results to infinite time.

Equation 26 also indicates that pseudo-isotherms can be generated even for irreversible adsorption if the maximum coverage is experimentally determined for a finite adsorption time as a function of bulk concentration. In this case, the long-time coverage increases proportionally to $n_b^{-1/3}$. For comparison, in the case of the Langmuir model describing reversible adsorption the true equilibrium coverage increases as n_b^{-1} for high coverage range.

It is also interesting to mention that the results derived from the standard RSA model by neglecting the bulk transport of molecules, depicted by the dashed line in Figure 6, significantly deviate from the results derived from the extended model. In particular, no well-pronounced linear regime (in respect to $t^{1/2}$) is observed in this case.

As far as experimental data are concerned, they are rather scarce for the diffusion controlled adsorption of fibrinogen at lower pH range, where the irreversible simultaneous adsorption mechanism is likely to appear. Some kinetic data can be extracted from in situ electrokinetic measurements of fibrinogen adsorption on mica at pH 3.5 in the presence of 10^{-2} M NaCl.[21] In that study, a unique functional relationship between the zeta potential of mica ζ (determined from the streaming potential measurements) and the adsorption time of fibrinogen t can be obtained. Using the theoretical approach discussed in ref 42, this dependence can be converted to the fibrinogen surface concentration vs the zeta potential relationship using the following expression

$$N = -\frac{N_{ch}}{C_i} \ln X(\zeta) \tag{27}$$

where N_{ch} is the scaling surface concentration, C_i is the dimensionless constant approaching for thin double-layers the limiting values of $C_i^0 = 10.2$ and $X_1(\zeta)$ is the normalized zeta potential given by

$$X(\zeta) = \frac{\zeta(t) - \zeta_p/\sqrt{2}}{\zeta_i - \zeta_p/\sqrt{2}} = \frac{\zeta(t) - \zeta_\infty}{\zeta_i - \zeta_\infty} \tag{28}$$

where $\zeta_\infty = \zeta_p/\sqrt{2}$ is the limiting zeta potential and ζ_p is the zeta potential of the protein in the bulk. It should be mentioned that the validity of eqs 27 and 28 for interpreting HSA adsorption on mica was confirmed in ref 42.

The experimental data obtained in ref 21 transformed to the N vs $t^{1/2}$ relationship are plotted in Figure 7. They are compared with theoretical predictions calculated by numerical solution of the diffusion equation with the blocking function given by eq 12 assuming the maximum coverage equal to 4500 μm^{-2} (corrected for the lateral electrostatic interactions). As can be observed, the experimental data agree with theoretical results calculated assuming the simultaneous adsorption over the entire range of surface concentrations. However, the precision of the streaming potential method becomes limited for higher surface concentration; therefore, one cannot precisely determine the jamming surface concentration of fibrinogen at this ionic strength.

This was determined in other experiments where suspensions of negatively charged latex particles (820 nm in diameter) were used.[43] The measurements were carried out at pH 3.5 and NaCl concentration varying from 10^{-3} to 0.15 M. Because of

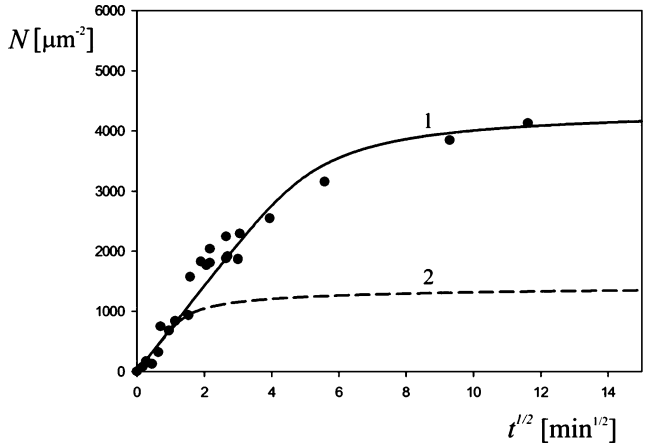

Figure 7. Kinetics of fibrinogen adsorption for the diffusion-controlled adsorption regime. The solid line 1 denote exact theoretical results calculated by solving the diffusion equation for the simultaneous adsorption regime, and the dashed line 2 denotes the results calculated for the side-on adsorption model. The points represent experimental results determined by streaming potential measurements for mica, pH 3.5 and 10^{-2} M NaCl.[21]

rapid kinetics of this process (characteristic time of the order of seconds) the jamming coverage could be precisely evaluated by the solution depletion method. These measurements revealed that the maximum coverage of fibrinogen on latex systematically increased with ionic strength attaining 3.6 mg m^{-2} for 0.15 M NaCl concentration. Using the effective hard-particle concept it was shown that this value corresponds the extrapolated jamming coverage of 4.12 mg m^{-2} for hard (noninteracting) molecules. This agrees with our calculations for the simultaneous adsorption model (see Table 3), which were performed for hard (noninteracting) molecules. The formation of dense brush-like fibrinogen monolayer on latex particles was also confirmed by DLS measurements of the hydrodynamic diameter of particles.[43]

Interestingly, the presence of a considerable amount of end-on oriented fibrinogen molecules was suggested by Santore and Wertz,[27] who observed a significant increase in the footprint area with time of molecules adsorbed on hydrophobized surfaces.

Analogously, in the work of Dyr et al.[44] it was unequivocally shown that the antibody binding to fibrinogen monolayers on gold strongly supports the hypothesis of end-on orientation of molecules. However, quantitative evidence of this were not provided.

In the work of Ortega–Vinuesa et al.[10,11] (fibrinogen adsorption on oxidized silicon substrate studied by ellipsometry) the maximum coverage of 3.8 mg m^{-2} was reported for pH = 4 and ionic strength of 0.05 M, which agrees with the result of Bratek et al.[43]

Precise kinetic measurements of fibrinogen adsorption on silicon and modified glass surfaces were performed by Wertz and Santore[26] using the *in situ* fluorescent TIRF technique. The measurements were made under convection-controlled transport conditions in a parallel-plate channel at pH = 7.4 (phosphate buffer). The bulk concentration of fibrinogen was varied 25, 50, and 100 ppm. For c_b = 25 mg L^{-1} the maximum coverage experimentally determined was 3.8 mg m^{-2}, which agrees fairly well with our theoretical predictions (by considering the correction for the lateral electrostatic interactions). However, for c_b = 50 an 100 mg L^{-1} noticeable

dx.doi.org/10.1021/la4012789 | *Langmuir* XXXX, XXX, XXX–XXX

deviations appeared for adsorption time longer than 1000 s since the coverage increased to the maximum value of 4.8 mg m^{-2}. Interestingly, an analogous result was obtained by Malmsten[25] using ellipsometry under diffusion transport conditions. These deviations can be most probably explained in terms of the formation of reversibly bound fibrinogen monolayer.

This experimental evidence confirm the utility of the simultaneous fibrinogen adsorption model for predicting adsorption kinetics and maximum coverage of fibrinogen on various surfaces at lower pH range. However, proving more refined aspects of this process, especially the transition from the side-on to end-on adsorption regime for higher coverage requires more sophisticated experimental techniques.

CONCLUDING REMARKS

The bead model of fibrinogen enabled one to quantitatively analyze its adsorption mechanisms on solid surfaces using the efficient random sequential adsorption approach.

The main results derived from these simulations are the surface blocking functions and jamming coverages for various adsorption mechanisms, *inter alia*, the side-on mechanisms with crossings, and the simultaneous side-on/end-on mechanism. In the latter case, it was shown that the side-on population of adsorbed molecules only dominates for surface concentration below 700 μm^{-2}. For higher surface concentration the end-on population prevails, which results in formation of brush-like fibrinogen monolayers. The predicted jamming coverage of this monolayer in the limit of high ionic strength is 7.34×10^3 μm^{-2} that corresponds to the coverage of 4.12 mg m^{-2} (for unhydrated molecule).

Experimental data obtained by electrokinetic measurements support the validity of this simultaneous adsorption mechanism for lower pH range where fibrinogen molecules are positively charged. Therefore, they can adsorb irreversibly on negatively charged surfaces both in the side-on and end-on orientations because of a large (negative) binding energy.

Additionally, the ellipsometric and TIRF measurements suggest that this simultaneous adsorption mechanism may be adequate for describing adsorption on hydrophobic surfaces at pH 7.4 and lower fibrinogen concentration. This can be so, because the binding energy is generally higher (more negative) for hydrophobic than for hydrophilic substrates. This facilitates an irreversible adsorption of fibrinogen under both side-on and end-on orientations.

On the other hand, the side-on mechanism analyzed before for the simplified Model A of fibrinogen[23] is plausible for adsorption at hydrophilic substrates and low ionic strength where the lateral repulsion among molecules makes the end-on adsorption improbable.

AUTHOR INFORMATION

Corresponding Author

*E-mail: ncadamcz@cyf-kr.edu.pl.

Notes

The authors declare no competing financial interest.

ACKNOWLEDGMENTS

This work was supported by the MNiSW Grant N N204 026438.

REFERENCES

(1) Ohta, R.; Saito, N.; Ishizaki, T.; Takai, O. Visualization of human plasma fibrinogen adsorbed on highly oriented pyrolytic graphite by scanning probe microscopy. *Surf. Sci.* **2006**, *600*, 1674−1678.

(2) Lewis, K. B.; Ratner, B. D. Imaging fibrinogen adsorbed on noble metal surfaces with scanning tunneling microscopy: correlation of images with electron spectroscopy for chemical analysis, secondary ion mass spectrometry, and radiolabeling studies. *Colloids Surf., B* **1996**, *7*, 259−269.

(3) Hantagan, R. R.; Simpson-Haidaris, P. J.; Francis, C. W.; Marder, V. J. Fibrinogen structure and physiology. In *Hemostasis and Thrombosis: Basic Principles and Clinical Practice*; Colman, R. W., Hirsh, J., Marder, V. J., Clowes, A. W., George, J. N., Eds.; Lippincott Williams & Wilkins: Philadelphia, 2000; pp 203−232.

(4) Le, M. T.; Dejardin, P. Simultaneous adsorption of fibrinogen and kininogen at a silica/solution interface. *Langmuir* **1998**, *14*, 3356−3364.

(5) Casals, E.; Verdaguer, A.; Tonda, R.; Galan, A.; Escolar, G.; Estelrich, J. Atomic force microscopy of liposomes bearing fibrinogen. *Bioconjugate Chem.* **2003**, *14*, 593−600.

(6) Hall, C. E.; Slayter, H. S. The fibrinogen molecule: its size, shape, and mode of polymerization. *J. Biophys. Biochem. Cytol.* **1959**, *5*, 11−16.

(7) Fowler, W. E.; Erickson, H. P. Trinodular structure of fibrinogen: Confirmation by both shadowing and negative stain electron microscopy. *J. Mol. Biol.* **1979**, *134*, 241−249.

(8) Weisel, J. W.; Stauffacher, C. V.; Bullitt, E.; Cohen, C. A model of fibrinogen: domains and sequance. *Science* **1985**, *230*, 1388−1391.

(9) Verklich, Y. J.; Gorkum, O. V.; Medved, L. V.; Nieuwenhuizen, W.; Weisel, S. W. Carboxyl-terminal portions of the alpha chains of fibrinogen and fibrin. Localization by electron microscopy and the effects of isolated alpha C fragments on polymerization. *J. Biol. Chem.* **1993**, *268*, 13577−13585.

(10) Ortega-Vinuesa, J. L.; Tengvall, P. I.; Lundstrom, I. Molecular packing of HSA, IgG, and fibrinogen adsorbed on silicon by AFM imaging. *Thin Solid Films* **1998**, *324*, 257−273.

(11) Ortega-Vinuesa, J. L.; Tengvall, P.; Lundström, I. , Aggregation of HSA, IgG, and fibrinogen on methylated silicon surfaces. *J. Colloid Interface Sci.* **1998**, *207*, 228−239.

(12) Sit, P. S.; Marchant, R. E. Surface-dependent conformations of human fibrinogen observed by atomic force microscopy under aqueous conditions. *Thromb. Haemost.* **1999**, *82*, 1053−1060.

(13) Marchin, K. L.; Berrie, C. L. Conformational changes in the plasma protein fibrinogen upon adsorption to graphite and mica investigated by atomic force microscopy. *Langmuir* **2003**, *19*, 9883−9888.

(14) Jung, S.-Y.; Lim, S.-M.; Albertorio, F. The Vroman effect: A molecular level description of fibrinogen displacement. *J. Am. Chem. Soc.* **2003**, *125*, 12782−12786.

(15) Tunc, S.; Maitz, M. F.; Steiner, G.; Vazquez, L.; Pham, M. T.; Salzer, R. In situ conformational analysis of fibrinogen adsorbed on Si surfaces. *Colloids Surf., B: Biointerfaces* **2005**, *42*, 219−225.

(16) Toscano, A.; Santore, M. M. Fibrinogen adsorption on three silica-based surfaces: conformation and kinetics. *Langmuir* **2006**, *22*, 2588−2597.

(17) http://www.rcsb.org

(18) Doolittle, R. F. Fibrinogen and fibrin. *Annu. Rev. Biochem.* **1984**, *53*, 195−229.

(19) Watt, K. W. K.; Takagi, T.; Doolittle, R. F. Amino acid sequence of the β chain of human fibrinogen: homology with the γ chain. *Proc. Natl. Acad. Sci. U.S.A.* **1978**, *75*, 1731−1735.

(20) Mosesson, M. W. Fibrinogen and fibrin structure and function. *Thromb. Haemost.* **2005**, *3*, 1894−1904.

(21) Wasilewska, M.; Adamczyk, Z. Fibrinogen adsorption on mica studied by AFM and in situ streaming potential measurements. *Langmuir* **2011**, *27*, 686−696.

(22) Adamczyk, Z.; Cichocki, B.; Ekiel-Jeżewska, M. L.; Słowicka, A.; Wajnryb, E.; Wasilewska, M. Fibrinogen conformations and charge in

electrolyte solutions derived from DLS and dynamic viscosity measurements. *J. Colloid Interface Sci.* **2012**, *385*, 244−257.
(23) Adamczyk, Z.; Barbasz, J.; Cieśla, M. Kinetics of fibrinogen adsorption on hydrophilic substrates. *Langmuir* **2010**, *26*, 11934−11945.
(24) Bai, Z.; Filiaggi, M. J.; Dahn, J. R. Fibrinogen adsorption onto 316L stainless steel, nitinol and titanium. *Surf. Sci.* **2009**, *603*, 839−846.
(25) Malmsten, M. Ellipsometry studies of protein layers adsorbed at hydrophobic syrfaces. *J. Colloid Interface Sci.* **1994**, *166*, 333−342.
(26) Wertz, Ch.F.; Santore, M. M. Effect of surface hydrophobicity on adsorption and relaxation kinetics of albumin and fibrinogen: single-species and competitive behaviour. *Langmuir* **2001**, *17*, 3006−3016.
(27) Santore, M. M.; Wertz, Ch.F. Protein spreading kinetics at liquid-solid interfaces via an adsorption probe method. *Langmuir* **2005**, *21*, 10172−10178.
(28) Kalasin, S.; Santore, M. M. Non-specific adhesion on biomaterial surfaces driven by small amounts of protein adsorption. *Colloids Surf., B: Biointerfaces* **2009**, *73*, 229−236.
(29) Adamczyk, Z.; Bratek-Skicki, A.; Dąbrowska, P.; Nattich-Rak, M. Mechanism of fibrinogen adsorption on latex particles determined by zeta potential and AFM measurements. *Langmuir* **2012**, *28*, 474−485.
(30) Adamczyk, Z.; Barbasz, J.; Cieśla, M. Mechanism of fibrinogen adsorption at solid substrates. *Langmuir* **2011**, *27*, 6868−6878.
(31) Hinrichsen, E. L.; Feder, J.; Jøssang, T. Geometry of random sequential adsorption. *J. Stat. Phys.* **1986**, *44*, 793−827.
(32) Schaaf, P.; Talbot, J. Surface exclusion effects in adsorption processes. *J. Chem. Phys.* **1989**, *91*, 4401−4409.
(33) Senger, B.; Voegel, J. C.; Schaaf, P. Irreversible adsorption of colloidal particles on solid substrates. *Colloids Surf., A* **2000**, *165*, 255−285.
(34) Evans, J. W. Random and cooperative sequential adsorption. *Rev. Mod. Phys.* **1993**, *65*, 1281.
(35) Talbot, J.; Tarjus, G.; van Tassel, P. R.; Viot, P. From car parking to protein adsorption: an overview of sequential adsorption process. *Colloids Surf., A* **2000**, *165*, 287−324.
(36) Vigil, R. D.; Ziff, R. M. Random sequential adsorption of unoriented rectangles onto a plane. *J. Chem. Phys.* **1989**, *91*, 2599−2602.
(37) Ricci, S. M.; Talbot, J.; Tarjus, G.; Viot, P. Random sequential adsorption of anisotropic particles I. Jamming limit and asymptotic behaviour. *J. Chem. Phys.* **1992**, *97*, 5219−5228.
(38) Viot, P.; Tarjus, G.; Ricci, S. M.; Talbot, J. Random sequential adsorption of anisotropic particles. II Low coverage kinetics. *J. Chem .Phys* **1992**, *97*, 5212−5218.
(39) Adamczyk, Z.; Weroński, P. Random sequential adsorption of spheroidal particles: kinetics and jamming limit. *J. Chem. Phys.* **1996**, *105*, 5562−5573.
(40) Adamczyk, Z. *Particles at Interfaces: Interactions, Deposition, Structure*; Academic Press, 2006.
(41) Adamczyk, Z. Modeling adsorption of colloid and proteins. *Curr. Opin. Colloid Interface Sci.* **2012**, *17*, 17.
(42) Dąbkowska, M.; Adamczyk, Z. Ionic strength effect in HSA adsorption on mica determined by streaming potential measurements. *Langmuir* **2012**, *28*, 15663.
(43) Bratek-Skicki, A.; Żelichowska, P.; Adamczyk, Z.; Cieśla, M. Human fibrinogen monolayers on latex particles: role of ionic strength. *Langmuir* **2013**, *29*, 3700−3710.
(44) Dyr, J. E.; Suttnar, J. Molecular arrangement of adsorbed fibrinogen molecules characterized by specific monoclonal antibodies and a surface plasmon resonance sensor. *Senso. Actuators, B* **1998**, *51*, 268−272.

dx.doi.org/10.1021/la4012789 | *Langmuir* XXXX, XXX, XXX−XXX